*energies*

MDPI

*Article*

# Leidenfrost Temperature on Trapezoidal Grooved Surface

**Qiwei Cao * and Yu Chen**

Graduate School of Frontier Sciences, The University of Tokyo, Kashiwanoha 5-1-5, Kashiwa City 277-8563, Chiba, Japan; chen@edu.k.u-tokyo.ac.jp
* Correspondence: qw.cao@scslab.k.u-tokyo.ac.jp; Tel.: +81-4-71364600

**Abstract:** In this study, we reported experimental results of a water droplet falling on trapezoidal grooved surfaces of heated silicon wafers with the groove width varied from 20 μm to 640 μm and the depth from 20 μm to 40 μm. Based on the observation of droplet dynamics captured by high-speed camera, we found that on the denser grooved surface, the maximum spreading diameter of the droplet perpendicular to the groove direction was smaller than that on the sparser grooved surface with the same groove depth. The residence time of the droplet on the denser grooved surface was shorter than that on the sparser grooved surface. The Leidenfrost point increased 50 °C with the groove width varied from 20 μm to 640 μm and decreased 10 °C when the depth was changed from 20 μm to 40 μm, which were higher than that on the smooth surface. Due to the deformation of the droplet during the droplet dynamics, it was difficult to calculate the heat transfer by measuring the droplet volume reduction rate. Based on the convective heat transfer from the grooved surface to the droplet, a Leidenfrost point model was developed. The results calculated by the model are in agreement with the experimental data.

**Keywords:** Leidenfrost temperature; trapezoidal grooved surface; convective heat transfer; capillary pressure; vapor convection

check for updates

**Citation:** Cao, Q.; Chen, Y. Leidenfrost Temperature on Trapezoidal Grooved Surface. *Energies* **2022**, *15*, 2875. https://doi.org/10.3390/en15082875

Academic Editors: Andrea De Pascale and Gabriela Huminic

Received: 16 March 2022
Accepted: 12 April 2022
Published: 14 April 2022

**Publisher's Note:** MDPI stays neutral with regard to jurisdictional claims in published maps and institutional affiliations.

**Copyright:** © 2022 by the authors. Licensee MDPI, Basel, Switzerland. This article is an open access article distributed under the terms and conditions of the Creative Commons Attribution (CC BY) license (https://creativecommons.org/licenses/by/4.0/).

## 1. Introduction

When liquid droplets impact on hot surfaces, they levitate on a vapor layer without wetting the surface, which insulates the droplets from the hot surface, and the heat transfer becomes lower, and the temperature that droplets levitate at is called the Leidenfrost point (LFP). The Leidenfrost effect on hot surfaces is a topic that has aroused a lot of interest in engineering fields, for example, micro-fabrication [1], electronic device cooling [2] and spray cooling [3]. Previous investigations showed that the Leidenfrost effect could be affected by many factors [4–6], including droplet properties [7], impact Weber number [8–11], thermal properties of hot surfaces [12], and surface structures [13–34]. Among micro-structures there are groove, hole, mesh, micro-roughness, porous wick, micro-structure fabricated by laser, pillars [25–33], and rig [35]. Compared to the LFP on the smooth surface, the LFP trend on these micro-structured surfaces is difficult summarize.

Duursma et al. [28] investigated the dynamics of droplets ranging in size from 8 to 24 μL impacted on a silicon surface with different micro-structured regions of square pillars. They correlated the experimental data for different droplet size, which showed that the Leidenfrost point was changed by up to 120 °C for pillar spacings from 10 to 100 μm. Yim et al. [36] experimentally measured the surface temperature and the internal flow fields of a droplet with initial radius of 3.7 mm, which showed the existence of critical radii on successive azimuthal mode transitions. Geraldi et al. [37] investigated the Leidenfrost temperature on discontinuous surfaces of stainless-steel meshes and found that with increasing the open area of the mesh, the Leidenfrost temperature was increased from 265 °C to 315 °C. Tenzer et al. [38] measured the Leidenfrost temperature during spray cooling of hot substrates and observed that the measured Leidenfrost temperature was dependent on the materials of both the liquid and the substrate. Lagubeau et al. [39]

investigated the Leidenfrost effect of a droplet on ratchets and showed that a directional thrust drove the levitating droplet. Teodori et al. [40] studied the heat transfer for the boiling of water on surfaces and observed that the heat flux increased almost linearly with the superheat for the superhydrophobic surfaces. Orejon et al. [41] reported the effect of ambient pressure on the wetting and levitating temperatures and indicated that the Leidenfrost temperature decreased with decreasing pressure at sub-atmospheric pressures.

The micro-structured surfaces fabricated by using Micro-electronic Mechanical System (MEMS) technics have been applied for increasing the LFP. Kim et al. [25] presented the influence of cylindrical micro-pillars on hydrophilic silicon surface with 15 μm height on the LFP, which was increased in the cases of sparser pillars located on the surface, compared to that on smooth surface, due to the intermittent liquid contact. They used heat conduction to calculate the heat transfer between the surface and the droplet at the LFP. Kwon et al. [26] dropped water droplets onto heated hydrophilic silicon surfaces textured with arrays of micro-scale silicon square pillars with the height of 10 μm. They also found that sparser rather than denser textures increased the Leidenfrost temperature, which could be controlled by modifying the size, distance and the height of micro-pillars on the surface. Zhang et al. [29] investigated the influence of pillar patterned surfaces with the height of 14 μm on the LFP on silicon wafers, which was superhydrophobic by coating with graphene nanosheets. They found that the high pillar would allow the droplet to contact the heated surface even if there was a vapor film. They explained that the gap between the micro-pillars exhausted the generated vapor and weakened the cushion effect. Kim et al. [32] gave the LFP changes on overheated micro-pillar surface with pillar height of 20 μm and different pillar density, and found that the moderate density pillar surface could enhance heat transfer due to the wetting condition. They also used the effective thermal conductivity to discuss the heat transfer. Tran et al. [42] impacted water droplets on a heated structured surface to investigate the influence of the micro-pillar height on the dynamic LFP, and found that the dynamic LFP decreased drastically when the pillar height increased from 2 μm to 8 μm. Kim et al. [43] conducted single droplet impinging experiments to measure dynamic Leidenfrost temperatures on surfaces with the uniformly distributed cylindrical micro-pillars in which the pillar pitches varied from 15 μm to 1000 μm. They found the Leidenfrost temperature increased monotonically as the pitch increased to a certain value but decreased above that pitch.

Kannan et al. [44] experimentally studied droplets' impact process on an unheated grooved surface and found that the geometry of grooved structure influenced the spreading process of impacting droplets on the grooved surface. Yan et al. [45] experimentally and numerically studied the dynamic and heat transfer characteristics of droplet impact on rectangular grooved surface and found that with the increase in impact velocity, the maximum spreading factor increased. Zhao et al. [11] investigated droplet impact dynamics with a different *We* number on a ridged surface of silicon wafer with the ridge height of 20 μm, and discussed the droplet directional rebounding on the gradient surface by using effective thermal conductivity. Maleprade et al. [46] studied the friction regimes of a droplet impacting on a ridged surface, which depended on the liquid speed and viscosity. Hays et al. [35] studied thermal transport to droplet falling on heated surface of super hydrophobicity with rib heights from 15 to 20 μm. They found that when the cavity fraction was increased, the Leidenfrost effect occurred at lower temperature. The heat transfer was calculated by the change in the droplet diameter during the droplet dynamics.

Compared to the studies of the influence of pillared surfaces on the Leidenfrost point, the grooved surface has received less attention. Since when a liquid droplet contacts hot grooved surfaces, the generated vapor directionally flows along the grooves, which is different from the rough surfaces or pillared surfaces. A Leidenfrost point model is needed in which the parameters of groove geometry are included. Therefore, in this study, the trapezoidal grooved structure on the surface of silicon wafer was selected to quantitatively investigate the Leidenfrost point trend of a droplet falling on the heated surface with various groove width and depth.

## 2. Experimental Setup

The micro-structure on the heated surface in our experiment was the trapezoidal groove (T-groove) with the slope angle of 55°, which was fabricated by using MEMS process on silicon wafers with the size of 30 × 30 mm, as shown in Figure 1. On each silicon wafer surface, there was only one type of T-groove structure with the same groove width and depth, and 16 silicon wafers were prepared with different groove widths and depths, as listed at Table 1; here, $b$ is the width of the groove, and $h$ is the depth of the groove, $a$ is the ridge width between two grooves, shown in Figure 1. In order to compare the effect of the grooved structure on droplet dynamics, a silicon wafer with smooth surface and an intrinsic contact angle of 58°, which means a hydrophilic surface, was used as reference.

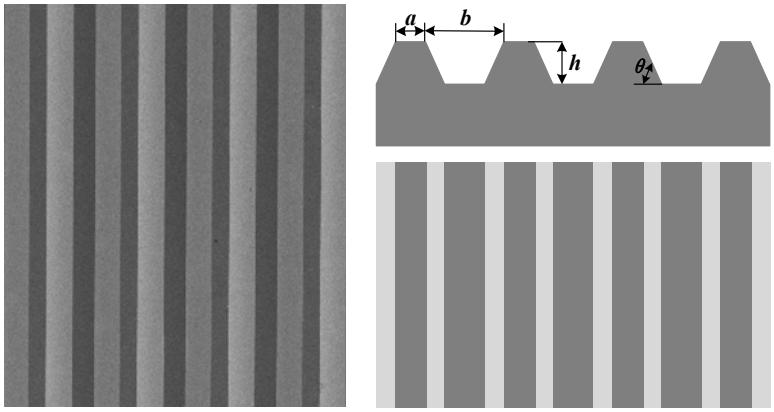



**Figure 1.** (**a**) The SEM image of the trapezoidal grooved structure on the surface of silicon wafers. The narrow dark region is the bottom of the groove. The shadow region is the slope surface of trapezoidal groove. The wider dark region is the bank of the groove; (**b**) Illustration of the trapezoidal grooved surfaces.

**Table 1.** The test number and parameters of trapezoidal grooved structures.

| Surface No. | Groove Width $w$ (μm) | Groove Depth $h$ (μm) |
|---|---|---|
| 1 | 20 | 20 |
| 2 | 40 | 20 |
| 3 | 80 | 20 |
| 4 | 120 | 20 |
| 5 | 160 | 20 |
| 6 | 240 | 20 |
| 7 | 320 | 20 |
| 8 | 640 | 20 |
| 9 | 20 | 40 |
| 10 | 40 | 40 |
| 11 | 80 | 40 |
| 12 | 120 | 40 |
| 13 | 160 | 40 |
| 14 | 240 | 40 |
| 15 | 320 | 40 |
| 16 | 640 | 40 |

The experimental apparatus consisted of an automatically controlled copper heater unit with a power of 1200 W and an automatic titrator, which was located above the center of the sample surface, as described in Figure 2. A single deionized water droplet was deposited on to the sample surface and its volume was automatically controlled. Three thermocouples were set near the center of the heater for tracking surface temperature, with a range of 100 °C to 500 °C to cover all evaporation regimes. The droplet dynamics on the surface of silicon wafer were recorded by high-speed camera recording system (Phantom).

The maximum spreading diameter on impact and residence time were measured for understanding and evaluating the LFP from the recorded graphs.

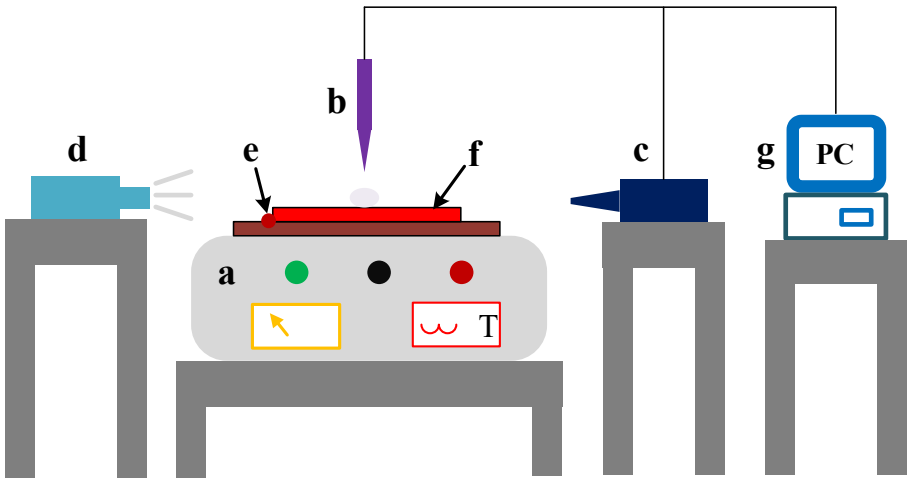



**Figure 2.** Schematic diagram of experimental apparatus: (**a**) Heater unit, (**b**) Micro-syringe, (**c**) CCD camera, (**d**) LED backlight, (**e**) Thermocouple temperature gauge, (**f**) Silicon wafer surface, (**g**) PC control unit.

In our experiment the deionized water droplet of 16 µL with $D_0$ the diameter of 3.12 mm was gently deposited on the surface of the silicon wafer from the PC-controlled micro-syringe. The droplet dynamics on each of the grooved surfaces with different widths and depths were recorded. Then the maximum spreading diameter and residence time were measured from the recorded graphs. The experimental procedure was that each silicon wafer was heated to the setting temperature, which was from 100 °C to 350 °C with the interval of 10 °C; then, we started the micro-syringe, and a droplet was released and deposited onto the heated surface. The Weber number is defined as

$$We = \rho_L V_L^2 D_0 / \sigma, \quad (1)$$

where the $\rho_L$ is the density of water liquid, $V_L$ is the velocity of the droplet, $D_0$ is the diameter of droplets and $\sigma_L$ is the surface tension of the droplet liquid. In our experiment, initial velocity of 0.3 m/s and Weber number of 3.9 were maintained throughout the whole experimental process.

## 3. Results

### *3.1. Observations*

The droplet dynamics were captured by a high-speed camera during the period in which the droplet contacted and bounded up from the heated surface. First, the droplet dynamics on the smooth surface were recorded, at 240 °C; the droplet was levitated on a vapor layer without wetting the surface, which means this temperature was the LFP on the smooth surface of the silicon wafer. When the surface temperature was increased to 250 °C, the droplet dynamics on the grooved surface presented different behavior. Figure 3 shows the droplet dynamics on the grooved surfaces at 250 °C with the groove depth of 20 µm and the width varied from 20 µm to 640 µm. When the droplet contacted the heated surface, the triple line of the droplet immediately started advancing wetting and reached its maximum spreading diameter at 6–7 ms.

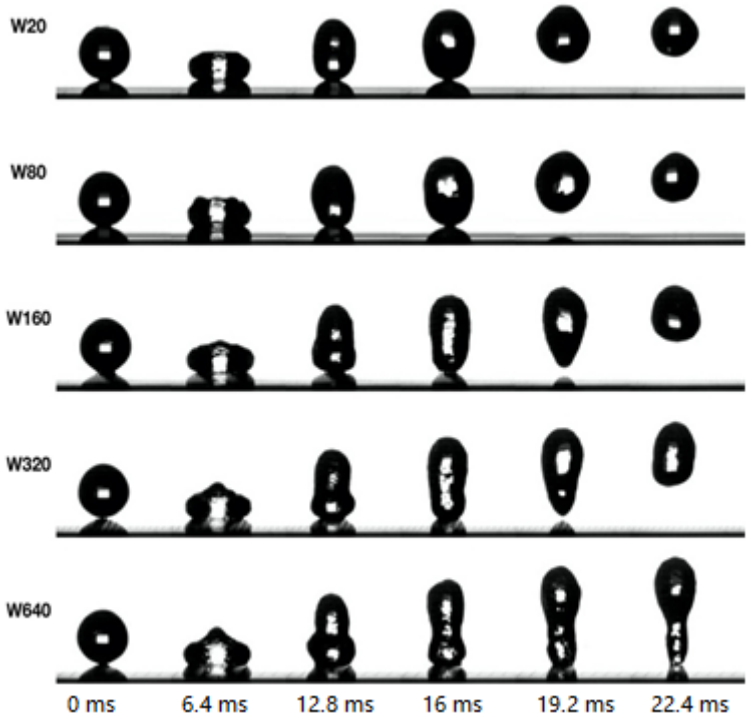



**Figure 3.** The droplet dynamics on T-grooved surfaces with depth of 20 μm and width of 20 μm to 640 μm at the surface temperature of 250 °C.

Then, the triple line started receding. From 16 to 24 ms the droplets were lifted up with strong evaporation at the interface, and rebounded. The droplet dynamics were intensified with the increase in the groove width. The rebounding behaviors were observed in the cases of the groove width being 40 μm and 80 μm, even if not stable. The droplet detached the surface at about 16 ms. When the groove width was increased from 120 μm to 640 μm, the droplet dynamics showed strong nucleation process from 12.8 ms, which means the vapor layer was not formed during the residence process. The residence time became longer, accompanied by a stronger nucleation effect. The droplet did not finish its rebound process at 22.4 ms, which means that it should be at a higher temperature for the droplet to reach film boiling.

The droplet dynamics on the grooved surface with a groove depth of 40 μm and a surface temperature of 250 °C are shown in Figure 4. Compared to those with a groove depth of 20 μm, as shown in Figure 3, the effects of the groove depth on the droplet dynamics were obvious. The rebounding process was faster in the case with the groove depth of 40 μm with the same width. The droplets on the surface with the groove width of 20 μm to 80 μm finished their rebounding process in less than 16 ms, a little bit shorter than that on the surface with the groove depth of 20 μm. Less agitation was observed during the process meaning that no obvious bubble nucleation with relatively smooth rebound was observed in the case of a deeper groove. The rebound process was finished within 22.4 ms on the surface with groove widths of 120 μm and 640 μm, showing less agitation with less nucleation, compared to those cases where the droplets did not finish their rebounding process at 22.4 ms on the surface with the groove depth of 20 μm.

### *3.2. Droplet Spreading*

On grooved surface, the spreading behavior of the droplet parallel to the groove direction is different from that perpendicular to the groove direction [38]. The spreading behavior of the droplet parallel to the groove direction is similar to that on a smooth surface, which has been investigated by many researchers. Here we focused on the spreading behavior of the droplet perpendicular to the groove direction.

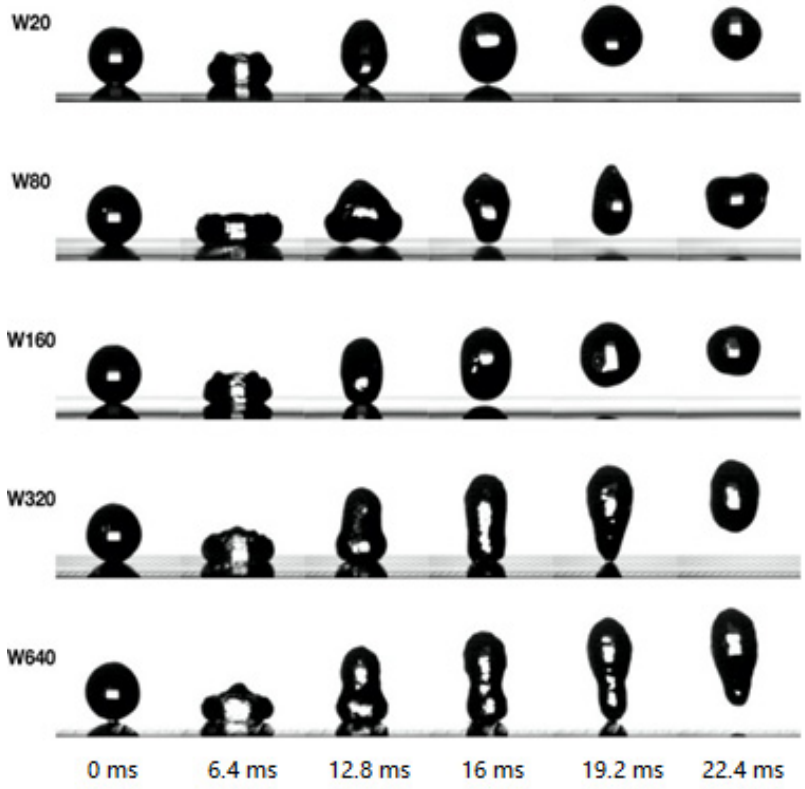



**Figure 4.** The droplet dynamics on T-grooved surfaces with depth of 40 μm and width of 20 μm to 640 μm at the surface temperature 250 °C.

In the following, the spreading factor means the spreading factor perpendicular to the groove direction. The maximum spreading factor is defined as that the maximum spreading diameter is divided by the initial droplet diameter, $D^*_{max} = \frac{D_{max}}{D_0}$; here, $D_{max}$ is the maximum spreading diameter of the droplet measured from the recorded graph during the droplet spreading process. Figure 5 shows the maximum spreading factor of the droplet, $D^*_{max}$ , on the T-grooved surface with the groove depth of 20 μm, which could be divided into two regions according to the groove width. In the range of 20 μm $\leq b \leq$ 80 μm, the $D^*_{max}$ was smaller than that in the range of 120 μm $\leq b \leq$ 640 μm, and the $D^*_{max}$ in sparser groove range decreased with the increase in groove width. It could be explained that in the denser groove range, non-permeable regime, in which the groove width was smaller, the impacting droplet could not penetrate into the grooves due to the stronger capillary pressure. The friction provided by capillary pressure and the rig contact points under the bottom of the droplet was strengthened with the smaller groove width, and the $D^*_{max}$ was smaller. At the groove width of 120 μm, the $D^*_{max}$ reached the maximum. In the sparser grooves range, permeable regime, due to the weaker capillary pressure, the impacting droplet could penetrate into the grooves, and the friction provided by capillary pressure and the rig contact points under the bottom of the droplet was weakened, and the friction at advancing triple line was reduced, and the $D^*_{max}$ was larger. With the increase in the groove width, the vapor pressure provided by vapor generation was increased inside the groove due to the penetration of droplet liquid into the grooves, and gave the droplet an upward movement, which reduced the speed up of the droplet horizontal movement, then the $D^*_{max}$ decreased with the increase in the groove width. The width of grooves affected the impact and maximum spreading factor of the droplet.

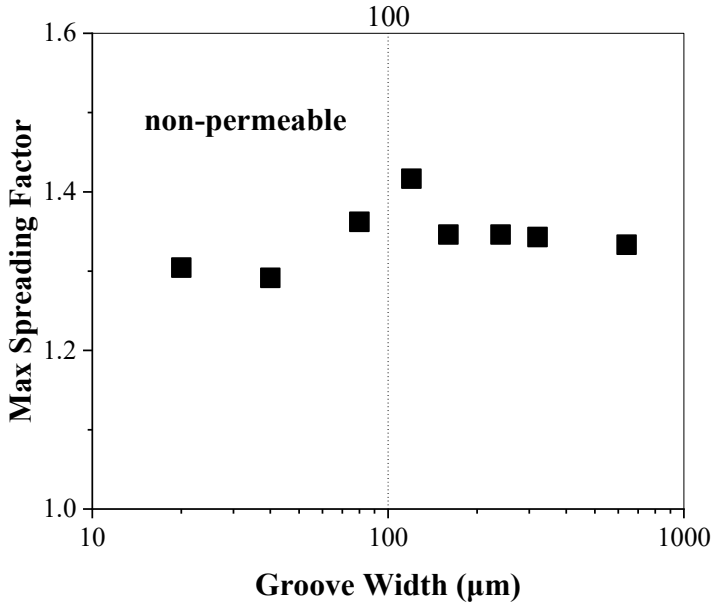



**Figure 5.** The maximum spreading factor of droplet on T-grooved surfaces with groove depth of 20 μm.

Figure 6 shows the maximum spreading factor of the droplet $D^*_{max}$ on the T-grooved surface with the groove depth of 40 μm, which also could be divided into two regions according to the groove width. In the range of 20 μm $\leq b \leq$ 120 μm, the $D^*_{max}$ was smaller than that in the range of 160 μm $\leq b \leq$ 640 μm, and the $D^*_{max}$ in sparser region decreased with the increase in groove width. The reason is the same as described in the case of the groove depth of 20 μm, which was the result of competition between capillary pressure and evaporation pressure. Compared to the result, as shown in Figure 5, the $D^*_{max}$ on deeper grooved surface was smaller. The groove depth affected the heat transferred from the surface to the droplet, and in the deeper groove the evaporation rate was stronger due to more heated surface, which increased the vapor pressure, and strengthened the upward movement of the droplet liquid, and then the $D^*_{max}$ became smaller. The depth of grooves affected the impact and maximum spreading factor of the droplet.

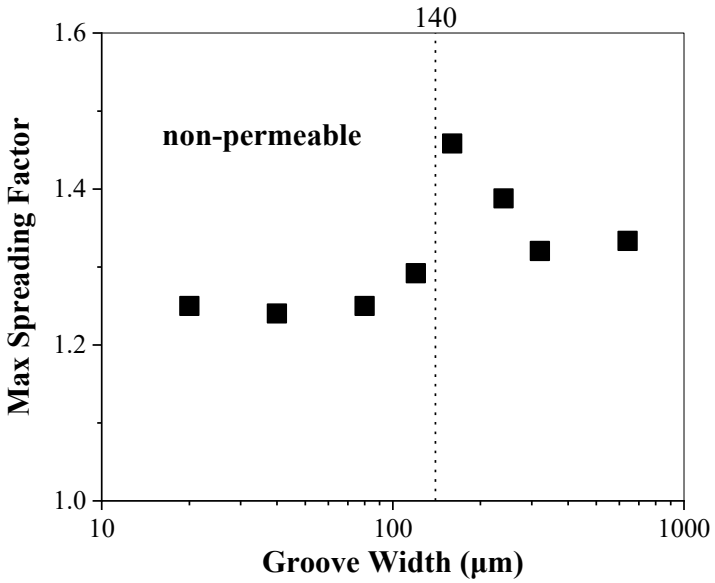



**Figure 6.** The maximum spreading factor of droplet on T-grooved surfaces with groove depth of 40 μm.

### *3.3. Droplet Rebounding*

The droplet residence time is defined as the duration from first contact with the surface to the first bounce from the heated surface $t_r$, which was measured using the high-speed visualization data. Figure 7 shows the droplet residence time on the surface with the T-groove surface with the depth of 20 μm, which could be divided into two regions according to the groove width. In the range of 20 μm $\leq b \leq$ 80 μm, the $t_r$ was shorter than that in the range of 120 μm $\leq b \leq$ 640 μm. It also could be explained that in the denser groove range, non-permeable regime, the impacting droplet could not penetrate into the grooves due to the stronger capillary pressure; therefore, the interaction between the droplet and the surface decreased, and the droplet showed stable rebounding dynamics, which induced shorter $t_r$. In the sparser grooves range, permeable regime, due to the weaker capillary pressure, the impacting droplet could penetrate into the groove, and contact the heated surface, the chance of bubble nucleation was increased, evaporation was strengthened, and the droplet became agitated, which induced longer $t_r$. The width of grooves affected the droplet rebounding process.

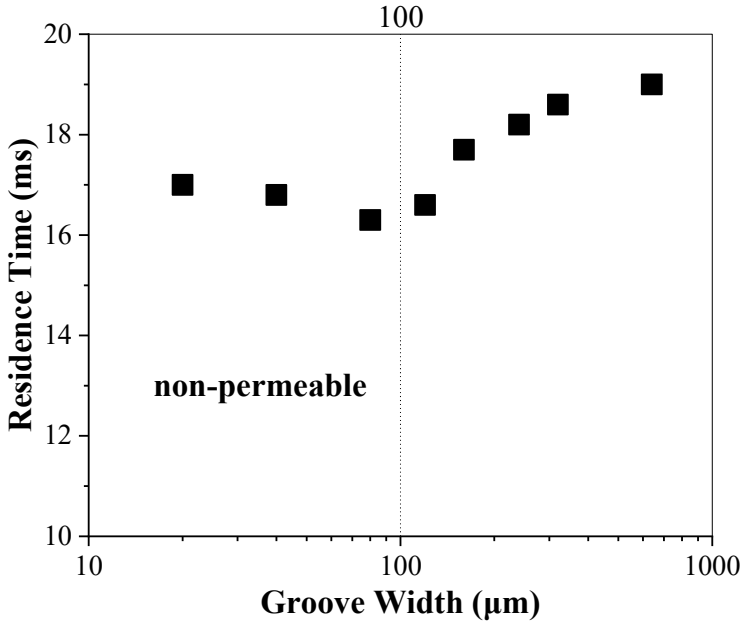



**Figure 7.** The residence time of droplet on T-grooved surfaces with groove depth of 20 μm.

Figure 8 shows the droplet residence time on the T-groove surface with the depth of 40 μm. In the range of 20 μm $\leq b \leq$ 120 μm, the $t_r$ was longer than that in the range of 160 μm $\leq b \leq$ 640 μm. It also could be the result of competition between capillary pressure, evaporation pressure and the chance of bubble nucleation. Compared to the results, as shown in Figure 7, the $t_r$ of the droplet on the deeper grooved surface was a little bit shorter. Due to a larger area of heated surface in the deeper groove, the evaporation was stronger and induced a little bit higher vapor pressure, which strengthened the upward movement of the droplet liquid; then, the $t_r$ was a little bit shorter. The depth of grooves affected the droplet rebounding process.

### *3.4. Leidenfrost Temperature*

When the surface temperature was increased from 150 °C to 230 °C, the droplet spreading on the surface was accompanied by typical nucleate boiling characteristics. When the surface temperature reached 240 °C, on the smooth surface, the droplet bounced without shattering and completely isolated the liquid surface contact, but it was not stable on the grooved surfaces.

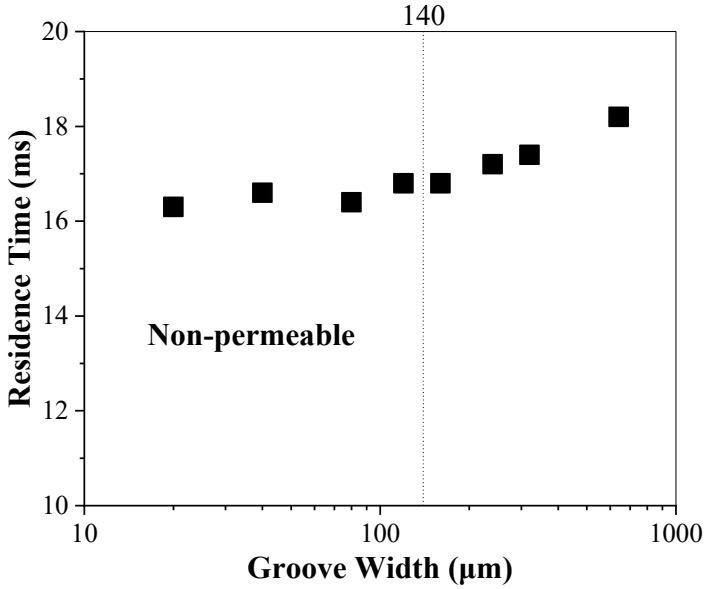



**Figure 8.** The residence time of droplet on T-grooved surfaces with groove depth of 40 μm.

On the surface with the groove depth of 20 μm, when the surface temperature was increased from 250 °C to 300 °C, the droplet spreading and rebounding gradually became stable and bounced without shattering, which means the droplet on the surfaces entered its Leidenfrost phenomena, and the surface temperature at this time was the Leidenfrost point. At the surface temperature of 250 °C, the droplet bounced stably and the droplet lifetime on the surface with the groove width of 20 μm was the longest. When the surface temperature reached 260 °C, the droplet rebounding became stable on the surface with the groove width of 40 μm. It could be seen from the Leidenfrost point trend that the Leidenfrost point on the grooved surface increase with the increase in the groove width.

The Leidenfrost point on the smooth surface was 240 °C and the Leidenfrost points on the grooved surfaces were higher than that value, influenced by the grooved structures on the heated surface. As shown in Figure 9, the Leidenfrost point was increased 50 °C when the groove width varied from 20 μm to 640 μm and decreased 10 °C when the depth was changed from 20 μm to 40 μm, which were higher than that on the smooth surface in the groove width range of 20 μm $\leq b \leq$ 640 μm and groove depth range of 20 μm and 40 μm.

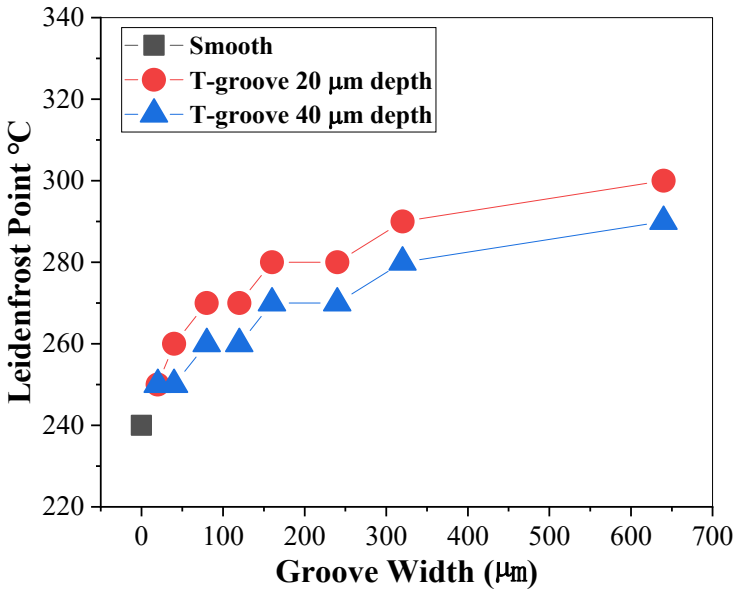



**Figure 9.** The LFPs on T-grooved surfaces with different groove width and depth.

## 4. Discussion

As shown in Figure 9, the Leidenfrost point increased with the increase in the groove width, but decreased with the increase in the groove depth, which was determined by the heat transfer between the heated surface and the droplet. In Kim's model [25], heat conduction was used to calculate the heat transfer for pillared surface. The effective thermal conductivity, which included the parameter of the height of pillar, was used by Kim et al. [32] to calculate the heat transfer for pillared surface. Zhao et al. [11] also used the effective thermal conductivity to calculate heat transfer on the gradient grooved surface. In Hays's study [35], convective heat transfer was considered to be the heat transfer mechanism from the heated surface to the droplet, but the droplet volume reduction rate during the dynamic process was used to calculate the heat transfer rate from the heated surface to the droplet. Since the deformation of the droplet was very large during the droplet dynamics, the droplet volume reduction rate was difficult to accurately measure in the experiments. Therefore, the modeling of the Leidenfrost point is difficult to derive from the droplet volume reduction rate.

The heat transfer to a Leidenfrost droplet causes vapor generation at the droplet bottom preventing direct contact between the droplet and the heated surface. The droplet thus levitates over the heated surface. For the minimum Leidenfrost droplet on the heated surface with the grooved structure, the contact schematic diagram of the droplet with the grooved surface is shown in Figure 10. The groove is filled with vapor generated due to the contact of the droplet bottom with the heated surface. In this study, the heat is transferred from the surface to the droplet via convection through the vapor layer. If the heat transferred from the grooved surface to the droplet is conduction, the heat transfer is $q = k\Delta T/h$; here, $h$ is the groove depth, $k$ is heat conduction coefficient of vapor, and $\Delta T$ is the temperature difference between the heated surface and the droplet bottom, which means that when the groove depth increases the heat transferred to the droplet decreases; then, the Leidenfrost temperature should be increased to levitate the droplet, which conflicts the experimental results, and the heat transfer rate by radiation is much smaller than that by heat conduction, and can be neglected.

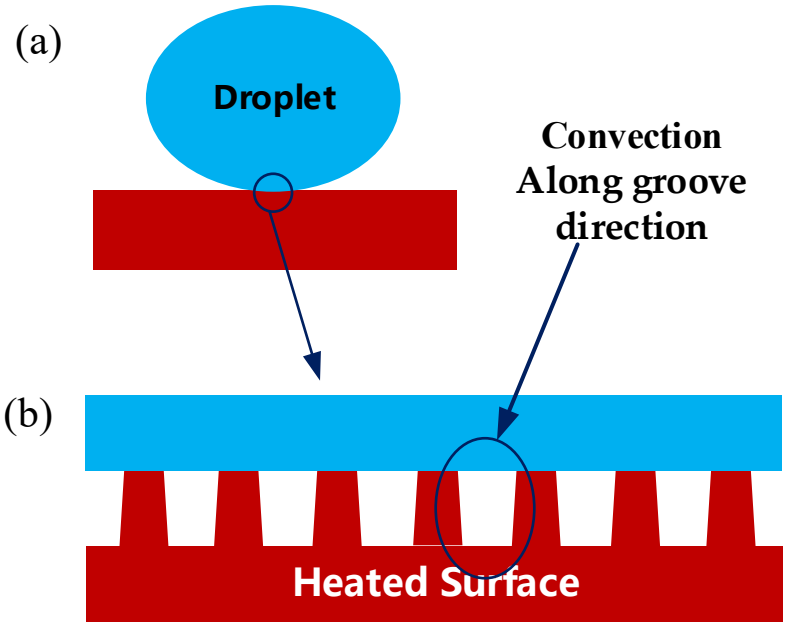



**Figure 10.** (**a**) The droplet falls on to the heated surface; (**b**) The contact schematic diagram of the droplet with the grooves and vapor on the grooved surface.

The natural convection perpendicular to the groove direction is impossible to establish in such a small size groove, since the Rayleigh number is very small. When the droplet liquid contacts the heated surface, and the evaporated vapor expands and flows inside the groove. The evaporation expansion is the force making the vapor flows. Here the forced convective heat transfer is borrowed to develop the heat transfer calculation. For the heat transfer of the micro-grooves on heated surface, which is considered as a micro-channel, the heat transfer Nusselt number $Nu$ is proportional to $CRe^n$ according to the reference [47]; here, n is 2 for simplifying the calculation. Since the $Nu$ number is obtained for a tube, and the channel is trapezoidal, the Nu number formula should be modified. Peng [48] considered the modification coefficients, one is $X_1 = (h/b)^{k_1}$ to modify ratio of the depth (h) to the width (b) of the channel, and the other is $X_2 = (p_w/D_h)^{k_2}$, here $p_w$ is wetting perimeter in the channel, and $D_h$ is hydraulic equivalent diameter, $k_1$ and $k_2$ are constant. Therefore, the modified $Nu$ number could be expressed as $Nu = CRe^n X_1 X_2$; here, C is constant.

The force balance of the droplet at the Leidenfrost point includes gravity, g, surface tension, $\Delta P_c$ and evaporation force, $\Delta P_v$. The surface tension provides a force downward and vapor pressure caused by evaporation provides upward force to levitate the droplet. The force caused by surface tension is much larger than the gravity force in our experiment, and the effect of gravity is negligible with respect to surface tension. The force caused by surface tension could be expressed as $\Delta P_c = 2\sigma/\mathrm{b}$. The force caused by evaporation can be expressed as $\Delta P_v = \Delta P$; here, $\Delta P$ is the pressure difference in the channel, which is equal to the friction force along the surface inside the channel, $\Delta P_v = 1/2 f \rho_v V_v^2$; here, $V_v$ is the velocity of the vapor along the channel, $\rho_v$ is the density of vapor, and $f$ is the friction coefficient of the vapor flowing inside the channel; here, $f = B/Re^{0.5}$ is employed. Therefore, the force balance is $\Delta P_c/\Delta P_v = 1$.

Additionally, the vapor flow from the channel is equal to the vapor generation from the bottom of the droplet, that is $\rho_v V_v hb = q_c/h_{fg}$, here $h_{fg}$ is the latent heat of liquid, $q_c$ is the heat transfer from the surface inside the channel to the bottom of the droplet by convection, which could be calculated by the $Nu$ number formation expressed as $q_c = k_v/D_h Nu \Delta T_L A$; here, $k_v$ is the heat conduction coefficient of vapor, $D_h$ is the hydraulic equivalent diameter of the channel, $A$ is the surface area of the channel, and $\Delta T_L$ is the temperature difference between the heated surface and the bottom of the droplet. At the Leidenfrost point, for the trapezoidal grooved surface on the heated silicon wafers, the surface superheat temperature $\Delta T_L$ can be derived and expressed as:

$$\Delta T_L = (Eb)^{\frac{2}{3}} \left(\frac{h}{b}\right)^{k1} \left(\frac{2h + b + a^2}{4hb}\right)^{k2} \left(\frac{2h(1 + \cot\theta) + b + a}{h(b + h\cot\theta)}\right), \quad (2)$$

Here, $E$ is the parameter summarized from the derivation of above formula, and $\theta$ is the angle of the slope of the trapezoidal groove. From the Leidenfrost point expression, which includes the groove depth ($h$) and width ($b$), it could be calculated that the Leidenfrost temperature increases with the increase in groove width, and decreases with the increase in groove depth, which is in agreement with the phenomena observed in our experiment.

The comparison of the calculated results of the normalized Leidenfrost point given by the expression (2) with experimental results are shown in Figures 11 and 12 for the grooved surface with the depths of 20 μm and 40 μm, respectively. From the calculated and the experimental results, the proposed mechanism of the vapor convective heat transfer inside the groove could be employed to explain that the Leidenfrost point increases with the increase in groove width, and decreases with the increase in groove depth.

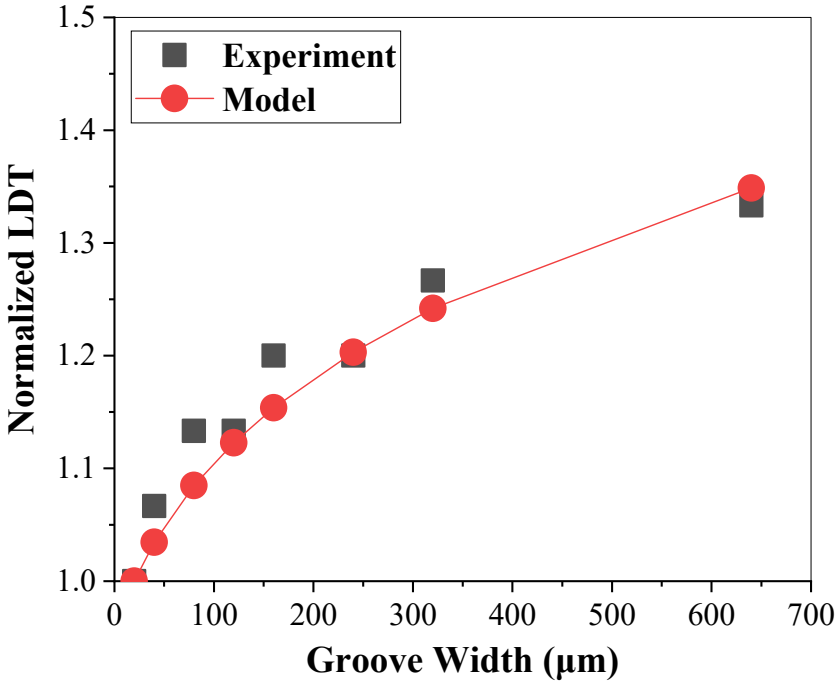



**Figure 11.** The comparison of normalized Leidenfrost point of modeling with the experimental results with T-groove depth of 20 μm.

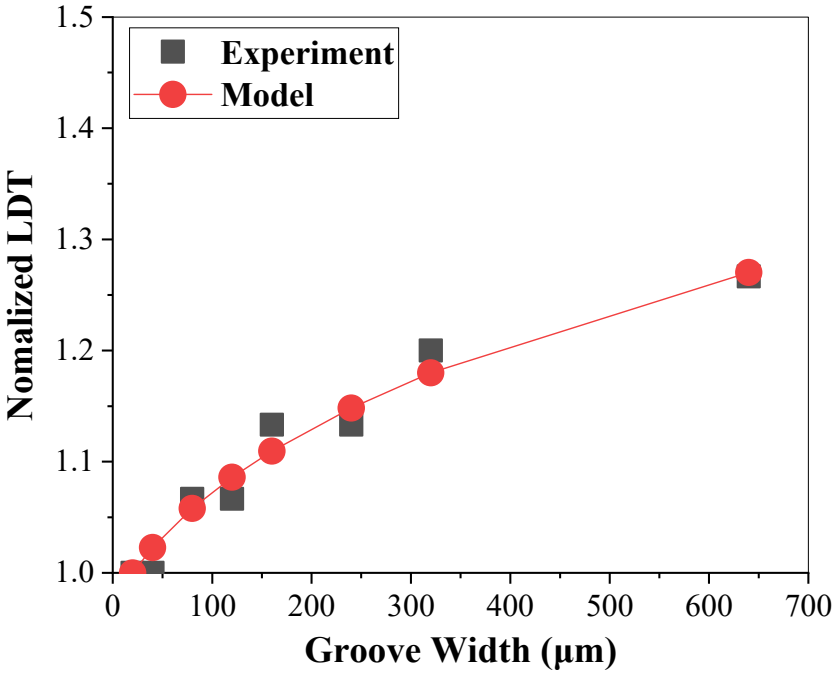



**Figure 12.** The comparison of normalized Leidenfrost point of modeling with the experimental results with T-groove depth of 40 μm.

## 5. Conclusions

The Leidenfrost point on the trapezoidal grooved surfaces of heated silicon wafers was experimentally studied and the droplet dynamics were visualized by high-speed camera, in which the droplet spreading diameter on impact and the residence time were measured. The summary of the findings is in the following.

When a water droplet falls onto the trapezoidal grooved surface of silicon wafers, on the denser grooved surface, the maximum spreading diameter perpendicular to the groove

direction was smaller than that on the sparser grooved surface with the same groove depth, and was larger than that on deeper grooved surface, which was caused by the competition of capillary pressure and evaporation pressure, affected by the groove width and depth. The residence time of the droplet on the denser grooved surface was shorter than that on the sparser grooved surface with the same groove depth.

The Leidenfrost point on the trapezoidal grooved surface was higher than that on the smooth surface, which was increased 50 °C with the groove width varied from 20 μm to 640 μm and decreased 10 °C when the depth was changed from 20 μm to 40 μm, meaning that higher surface temperature is acquired to reach film boiling for wider groove, and lower temperature is acquired to reach film boiling for deeper groove, which could be used to control the boiling behavior.

The heat transferred from the heated surface inside the groove to the droplet bottom at Leidenfrost point was induced by convection, in which the generated vapor was released into the groove and flows along the groove. Based on the vapor convection, the heat transfer from the heated surface to the droplet at the Leidenfrost point was calculated, and a model of Leidenfrost point for the trapezoidal grooved surface of silicon wafers was developed and the calculated results were in agreement with the experimental results, which could be used to explain the observed experimental phenomena.

The Leidenfrost point trend on the trapezoidal grooved surface of silicon wafers was studied and the results could be used to design the grooves to control the boiling behaviors on the structured surfaces. Since several factors will influence the Leidenfrost temperature, in the future, the influence of surface material and droplet liquid properties with grooved structures will be investigated.

**Author Contributions:** Methodology, supervision, writing—review and editing, Y.C.; investigation, formal analysis, writing—original draft preparation, Q.C. All authors have read and agreed to the published version of the manuscript.

**Funding:** This research received no external funding.

**Institutional Review Board Statement:** Not applicable.

**Informed Consent Statement:** Not applicable.

**Data Availability Statement:** Not applicable.

**Conflicts of Interest:** The authors declare no conflict of interest.

## References

1. Yoo, J.Y. Recent studies on fluid flow and heat transfer in thermal microdevices. *Nanoscale Microscale Thermophys. Eng.* **2006**, *10*, 67–81. [CrossRef]
2. Selvam, R.P.; Lin, L.; Ponnappan, R. Direct simulation of spray cooling: Effect of vapor bubble growth and liquid droplet impact on heat transfer. *Int. J. Heat Mass Transf.* **2006**, *49*, 4265–4278. [CrossRef]
3. Zhang, Z.; Jiang, P.-X.; Christopher, D.M.; Liang, X.-G. Experimental investigation of spray cooling on micro-, nano- and hybrid-structured surfaces. *Int. J. Heat Mass Transf.* **2015**, *80*, 26–37. [CrossRef]
4. Fukai, J.; Shiiba, Y.; Yamamoto, T.; Miyatake, O.; Poulikakos, D.; Megaridis, C.M.; Zhao, Z. Wetting effects on the spreading of a liquid droplet colliding with a flat surface: Experiment and modeling. *Phys. Fluids* **1995**, *7*, 236–247. [CrossRef]
5. Bertola, V. An impact regime map for water drops impacting on heated surfaces. *Int. J. Heat Mass Transf.* **2015**, *85*, 430–437. [CrossRef]
6. Van Limbeek, M.A.; Shirota, M.; Sleutel, P.; Sun, C.; Prosperetti, A.; Lohse, D. Vapor cooling of poorly conducting hot substrates increases the dynamic Leidenfrost temperature. *Int. J. Heat Mass Transf.* **2016**, *97*, 101–109. [CrossRef]
7. Cui, Q.; Chandra, S.; McCahan, S. The Effect of Dissolving Salts in Water Sprays Used for Quenching a Hot Surface: Part 2—Spray Cooling. *J. Heat Transf.* **2003**, *125*, 333–338. [CrossRef]
8. Gradeck, M.; Seiler, N.; Ruyer, P.; Maillet, D. Heat transfer for Leidenfrost drops bouncing onto a hot surface. *Exp. Therm. Fluid Sci.* **2013**, *47*, 14–25. [CrossRef]
9. Hamdan, K.S.; Kim, D.-E.; Moon, S.-K. Droplets behavior impacting on a hot surface above the Leidenfrost Temperature. *Ann. Nucl. Energy* **2015**, *80*, 338–347. [CrossRef]
10. Villegas, L.R.; Tanguy, S.; Castanet, G.; Caballina, O.; Lemoine, F. Direct numerical simulation of the impact of a droplet onto a hot surface above the Leidenfrost temperature. *Int. J. Heat Mass Transf.* **2017**, *104*, 1090–1109. [CrossRef]

11. Zhao, D.; Sun, Y.; Liu, C.; Zhan, H.; Wang, M.; Liu, J.; Liu, Y. Temperature-regulated directional bounce of impacting droplets on gradient Grooves. *Surf. Coat. Technol.* **2018**, *356*, 132–137. [CrossRef]
12. Wu, R.; Lamini, O.; Zhao, C.Y. Leidenfrost temperature: Surface thermal diffusivity and effusivity effect. *Int. J. Heat Mass Transf.* **2021**, *168*, 120892. [CrossRef]
13. Arter, J.M.; Cleaver, D.J.; Takashina, K.; Rhead, A.T. Self-propelling Leidenfrost droplets on a variable topography surface. *Appl. Phys. Lett.* **2018**, *113*, 243704. [CrossRef]
14. Dubnack, O.; Kunz, C.; Graf, S.; Muller, F.A. Laser-induced Leidenfrost surfaces. *Appl. Surf. Sci.* **2020**, *532*, 147407. [CrossRef]
15. Wang, G.; McDonough, J.R.; Zivkovic, V.; Long, T.; Wang, S. From Thermal Energy to Kinetic Energy: Droplet Motion Triggered by the Leidenfrost Effect. *Adv. Mater. Interfaces* **2021**, *8*, 2001249. [CrossRef]
16. Jia, Z.; Chen, M.; Zhu, H. Reversible self-propelled Leidenfrost droplets on ratchet surfaces. *Appl. Phys. Lett.* **2017**, *110*, 091603. [CrossRef]
17. Lee, D.J.; Song, Y.S. Anomalous water drop bouncing on a nanotextured surface by the Leidenfrost levitation. *Appl. Phys. Lett.* **2016**, *108*, 201604. [CrossRef]
18. Sajadi, S.M.; Irajizad, P.; Kashyap, V.; Farokhnia, N.; Ghasemi, H. Surfaces for high heat dissipation with no Leidenfrost limit. *Appl. Phys. Lett.* **2017**, *111*, 021605. [CrossRef]
19. Zhong, L.; Guo, Z. Effect of surface topography and wettability on the Leidenfrost effect. *Nanoscale* **2017**, *9*, 6219–6236. [CrossRef]
20. Lee, G.C.; Kang, J.; Park, H.S.; Moriyama, K.; Kim, S.H.; Kim, M.H. Induced liquid-solid contact via micro/nano multiscale texture on a surface and its effect on the Leidenfrost temperature. *Exp. Therm. Fluid Sci.* **2017**, *84*, 156–164. [CrossRef]
21. Lee, G.C.; Kim, S.H.; Kang, J.; Kim, M.H.; Jo, H. Leidenfrost temperature on porous wick surfaces: Decoupling the effects of the capillary wicking and thermal properties. *Int. J. Heat Mass Transf.* **2019**, *145*, 118809. [CrossRef]
22. Kim, S.H.; Ahn, H.S.; Kim, J.; Kim, M.H.; Park, H.S. Experimental study of water droplets on over-heated nano/microstructured zirconium surfaces. *Nucl. Eng. Des.* **2014**, *278*, 367–376. [CrossRef]
23. Kruse, C.; Somanas, I.; Anderson, T.; Wilson, C.; Zuhlke, C.; Alexander, D.; Gogos, G.; Ndao, S. Self-propelled droplets on heated surfaces with angled self-assembled micro/nanostructures. *Microfluid. Nanofluid.* **2015**, *18*, 1417–1424. [CrossRef] [PubMed]
24. Hassebrook, A.; Kruse, C.; Wilson, C.; Anderson, T.; Zuhlke, C.; Alexander, D.; Gogos, G.; Ndao, S. Effects of Droplet Diameter and Fluid Properties on the Leidenfrost Temperature of Polished and Micro/Nanostructured Surfaces. *J. Heat Trans.* **2016**, *138*, 051501. [CrossRef]
25. Kim, H.; Truong, B.; Buongiorno, J.; Hu, L.-W. On the effect of surface roughness height, wettability, and nanoporosity on Leidenfrost phenomena. *Appl. Phys. Lett.* **2011**, *98*, 083121. [CrossRef]
26. Kwon, H.; Bird, J.C.; Varanasi, K.K. Increasing Leidenfrost point using micro-nano hierarchical surface structures. *Appl. Phys. Lett.* **2013**, *103*, 201601. [CrossRef]
27. Wang, J.; Do-Quang, M.; Cannon, J.J.; Yue, F.; Suzuki, Y.; Amberg, G.; Shiomi, J. Surface structure determines dynamic wetting. *Sci. Rep.* **2014**, *5*, 8474. [CrossRef]
28. Duursma, G.; Kennedy, R.; Sefiane, K.; Yu, Y. Leidenfrost Droplets on Microstructured Surfaces. *Heat Transf. Eng.* **2016**, *37*, 1190–1200. [CrossRef]
29. Zhang, W.; Yu, T.; Fan, J.; Sun, W.; Cao, Z. Droplet impact behavior on heated micro-patterned Surfaces. *J. Appl. Phys.* **2016**, *119*, 114901. [CrossRef]
30. Talari, V.; Behar, P.; Lu, Y.; Haryadi, E.; Liu, D. Leidenfrost drops on micro/nanostructured surfaces. *Front. Energy* **2018**, *12*, 22–42. [CrossRef]
31. Chen, M.; Jia, Z.; Zhang, T.; Fei, Y. Self-propulsion of Leidenfrost droplets on micropillared hot surfaces with gradient wettability. *Appl. Surf. Sci.* **2018**, *433*, 336–340. [CrossRef]
32. Kim, S.H.; Lee, G.; Kim, H.M.; Kim, M.H. Leidenfrost point and droplet dynamics on heated micropillar array surface. *Int. J. Heat Mass Transf.* **2019**, *139*, 1–9. [CrossRef]
33. Park, J.; Kim, D.E. Dynamic Leidenfrost temperature of saturated water drops on textured surfaces. *Int. J. Heat Mass Transf.* **2020**, *150*, 119298. [CrossRef]
34. Dodd, L.E.; Agrawal, P.; Geraldi, N.R.; Xu, B.B.; Wells, G.G.; Martin, J.; Newton, M.I.; McHale, G.; Wood, D. Planar selective Leidenfrost propulsion without physically structured substrates or walls. *Appl. Phys. Lett.* **2020**, *117*, 081601. [CrossRef]
35. Hays, R.; Maynes, D.; Crockett, J. Thermal transport to droplets on heated superhydrophobic substrates. *Int. J. Heat Mass Transf.* **2016**, *98*, 70–80. [CrossRef]
36. Yim, E.; Bouillant, A.; Quéré, D.; Gallaire, F. Stability of Leidenfrost drop inner flows. *arXiv* **2020**, arXiv:2012.10408.
37. Geraldi, N.R.; McHale, G.; Xu, B.B.; Wells, G.G.; Dodd, L.E.; Wood, D.; Newton, M.I. Leidenfrost transition temperature for stainless steel meshes. *Mater. Lett.* **2016**, *176*, 205–208. [CrossRef]
38. Tenzer, F.M.; Hofmann, J.; Roisman, I.V.; Tropea, C. Leidenfrost temperature in sprays: Role of the substrate and liquid properties. *arXiv* **2020**, arXiv:2001.05426.
39. Lagubeau, G.; Merrer, M.L.; Clanet, C.; Quéré, D. Leidenfrost on a ratchet. *Nat. Phys.* **2011**, *7*, 395–398. [CrossRef]
40. Teodori, E.; Valente, T.; Malavasi, I.; Moita, A.S.; Marengo, M.; Moreira, A.L.N. Effect of extreme wetting scenarios on pool boiling conditions. *Appl. Therm. Eng.* **2017**, *115*, 1424–1437. [CrossRef]
41. Orejon, D.; Sefiane, K.; Takata, Y. Effect of ambient pressure on Leidenfrost temperature. *Phys. Rev. E* **2014**, *90*, 053012. [CrossRef] [PubMed]

42. Tran, T.; Staat, H.J.J.; Susarrey-Arce, A.; Foertsch, T.C.; van Houselt, A.; Gardeniers, H.J.G.E.; Prosperetti, A.; Lohse, D.; Sun, C. Droplet impact on superheated micro-structured surfaces. *Soft Matter* **2013**, *9*, 3272–3282. [CrossRef]
43. Kim, D.E. Dynamic Leidenfrost temperature behaviors on uniformly distributed micropillars. *Exp. Therm. Fluid Sci.* **2020**, *111*, 109954. [CrossRef]
44. Kannan, R.; Sivakumar, D. Drop impact process on a hydrophobic grooved surface. *Colloids Surf. A Physicochem. Eng. Asp.* **2008**, *317*, 694–704. [CrossRef]
45. Yan, Z.; Li, Y. A comprehensive study of dynamic and heat transfer characteristics of droplet impact on micro-scale rectangularg Grooved surface. *Energies* **2018**, *11*, 1390. [CrossRef]
46. Maleprade, H.; Keiser, A.; Clanet, C.; Quéré, D. Friction properties of superhydrophobic ridges. *J. Fluid Mech.* **2020**, *890*, A19. [CrossRef]
47. Choi, S.B.; Barron, R.F.; Warrington, R.O. Fluid Flow and Heat Transfer in Microtubes. In *Micromechanical Sensors, Actuators, and Systems*; ASME: New York, NY, USA, 1991; Volume 32.
48. Peng, X.F.; Peterson, G.P. Convective heat transfer and flow friction for water flow in microchannel structures. *Int. J. Heat Mass Transf.* **1996**, *39*, 2599–2608. [CrossRef]